Creation and decay of high-energy phonons in anisotropic systems of low-energy phonons in superfluid helium

I. N. Adamenko,[1] Yu. A. Kitsenko,[2] K. E. Nemchenko,[1] V. A. Slipko,[1] and A. F. G. Wyatt[3,*]
[1]*Karazin Kharkov National University, Svobody Square 4, Kharkov, 61077, Ukraine*
[2]*Akhiezer Institute for Theoretical Physics, National Science Center, Kharkov Institute of Physics and Technology, National Academy of Sciences of Ukraine, 1, Academicheskaya Street, Kharkov, 61108, Ukraine*
[3]*School of Physics, University of Exeter, Exeter EX4 4QL, United Kingdom*
(Received 17 November 2005; revised manuscript received 26 January 2006; published 5 April 2006)

The creation and decay rates of high-energy phonons (*h*-phonons) in anisotropic systems of low-energy phonons (*l*-phonons), are calculated using the exact distribution function for anisotropic phonon systems in superfluid helium. The angular distribution of created *h*-phonons is then found, and it is shown that the solid angle occupied by created *h*-phonons is always less than the solid angle occupied by *l*-phonons, as is found experimentally. The evolution of the *l*-phonon pulse, due to *h*-phonon creation, is analyzed. This leads to an explanation of the measured dependence of the *l*-phonon signal on heater power.

DOI: 10.1103/PhysRevB.73.134505 PACS number(s): 67.70.+n, 68.08.−p, 62.60.+v

I. INTRODUCTION

Anisotropic phonon systems can be readily created in superfluid helium: for example a pulse of phonons travelling along the z axis is an extremely anisotropic distribution of phonons in momentum space. When this anisotropy is coupled with the anomalous phonon dispersion in liquid helium, some very interesting phenomena occur. For example, a single short phonon pulse injected into liquid helium develops into two pulses after propagating around 10 mm,[1,2] furthemore one pulse consists of low energy phonons and the other of high energy phonons.[2] Experiments have shown that the high energy phonons are created from the low energy phonons as the pulse propagates,[3] and there is a good theoretical understanding of this effect.[4] In essence, the low energy phonons (*l*-phonons) are strongly interacting, by three phonon processes (3PP),[5,6] and are in dynamic equilibrium, and the high energy phonons (*h*-phonons) are created by higher order scattering, four phonon processes (4PP),[7,8] from the *l*-phonons. For short pulses, the details of the dispersion curve cause an energy ratchet: *h*-phonons are created from low energy phonons, and once created they do not decay. The equilibrium assumed for the *l*-phonons does not extend to the *h*-phonons in this case. This unusual process is a result of the anisotropy; in an isotropic system it cannot occur.

Although a good deal of theoretical progress has been made to explain the behavior of anisotropic phonon systems in He II,[8–10] we now have a new way of treating them which avoids the central approximation that was made previously: the "Bose-Einstein cone" distribution function.[8–10] We can now use a distribution function which correctly solves the kinetic equation for an anisotropic system in dynamic equilibrium.[11] The distribution function is defined in terms of two variables, the temperature T and the "drift" velocity $\mathbf{u}$ of the system. This contrasts with the distribution function for an isotropic system in equlibrium which only has one variable T.

Previously we used the Bose-Einstein cone approximation,[8–10] in which the anisotropic system is taken to be a conical segment of an isotropic distribution at temperature T_p. The two variables in this case are T_p and the cone angle θ_c of the segment. While this remains a useful and intuitive way of visualizing the anisotropic system, it has a serious failing: the cone angle is constant in time. This cannot be correct when the anisotropic system creates and loses *h*-phonons predominantly along the z axis, which it does as we shall show below. The loss of energy and axial momentum by the l-phonons causes the angular distribution of their momenta to increase because momentum is conserved overall; in terms of the *B-E* cone approximation, the cone angle increases, which contradicts the approximation.

This new formalism has important consequences which are the subject of this paper. It enables us to solve a fundamental problem which has not been possible before. Experimentally it is found that the *l*-phonon energy density, after the pulse has propagated 17 mm, is approximately proportional to the heater pulse power that created it.[12] At first sight this does not seem unreasonable or remarkable but on closer inspection there is problem. As the short pulse propagates it loses energy density by *h*-phonon creation; the *h*-phonons have a lower group velocity than the pulse and so are lost from the pulse. The creation rate of *h*-phonons is strongly temperature dependent and decreases to a very small value when T_p has fallen to ~ 0.7 K.[10] This means that after a long path length of 17 mm, the temperature of the pulse $T_p \sim 0.7$ K and is independent of the initial temperature.

Now the energy density of the *l*-phonon pulse is $\propto \Omega_c T_p^4$,[10] where the solid angle of the occupied states in momentum space is related to the cone angle by $\Omega_c = 2\pi(1-\cos\theta_c)$. So if the final energy density is proportional to the heater power W, then the final value of $\Omega_c T_p^4$ must be also proportional to W. As T_p is independent of W, this implies that the initial cone angle of the distribution created by the heater, must increase roughly proportional to W.[12] The puzzle is then: why should the initial angular distribution depend on heater power? We are forced to this question because in the *B-E* cone approximation, once the cone angle is set initially, it remains constant.

From the conservation of momentum argument given above, it is unreasonable to assume θ_c is constant. We must find a different explanation for the experimental result, that the energy density is proportional to W. We propose that the angular distribution of the momentum increases as the pulse propagates. In this scenario, the final value of Ω_c is again roughly proportional to W, but now it is because Ω_c has increased during the propagation of the pulse, and the amount of the increase is roughly proportional to W. The analysis in this paper shows that the angular distribution of momentum does increase as the pulse propagates. Surprisingly the temperature T increases too (but not T_p, which decreases), but the energy density decreases as it must.

In this paper the exact local-equilibrium distribution function of phonons in a pulse[11] is used to calculate the creation and decay rate of h-phonons. The phonon dispersion curve and its effect on phonon scattering is discussed in Sec. II. The kinetic equation for the distribution function of the h-phonons is found in Sec. III. The creation and decay rates of h-phonons, at any angle to the propagation direction, in the l-phonon pulse, are derived in Sec. IV. It allows us to obtain the angular dependence of the h-phonon creation processes in Sec. V. This explains why the h-phonons are more concentrated along the anisotropy axis of the system than the l-phonons. The evolution of the l-phonon pulse, caused by h-phonon creation, is described in Sec. VI. This enables us to explain why the l-phonon signal increases with increasing heater power.

II. PHONON DISPERSION AND SCATTERING

The dispersion relation is crucially important for phonon-phonon interactions in superfluid helium (He II) because of the initial upward dispersion.[13,14] The dispersion relation can be written as

$$\varepsilon = cp[1 + \psi(p)], \tag{1}$$

where c is sound velocity and ε and p are the phonon energy and momentum. $\psi(p)$ is a function which describes the deviation of the spectrum from linearity which is small $[|\psi(p)| \ll 1]$, but it nevertheless completely determines the type and strength of phonon interactions.

When $p < p_c$ the function $\psi > 0$ (anomalous dispersion). In this case the conservation laws of energy and momentum allow processes which do not conserve the number of phonons. The fastest of these processes is the three-phonon process in which one phonon decays into two or two interacting phonons combine into one.

When $p > p_c$ the function $\psi < 0$. In this case the dispersion is normal and 3PP are prohibited by the conservation laws of energy and momentum, and there is no spontaneous phonon decay. Then the fastest processes are 4PP. There is a strong inequality between the 3PP and 4PP scattering rates

$$\nu_{3\mathrm{PP}} \gg \nu_{4\mathrm{PP}}. \tag{2}$$

This causes the phonons in superfluid helium to break up into two subsystems: a subsystem of h-phonons with $p > p_c$ in which equilibrium is attained relatively slowly, and a subsystem of l-phonons with $p < p_c$ in which equilibrium is attained relatively quickly. On the time scales involved in the phonon propagation, equilibrium in a subsystem of l-phonons occurs instantaneously.

Anisotropic phonon systems are usually created in superfluid helium at such a low temperature that the thermal excitations can be neglected. A short heat pulse, of duration t_p, creates a l-phonon pulse which moves in the "phonon vacuum" with a velocity nearly equal to c.[15] In real space, the transverse dimensions of this highly anisotropic system near the heater, are about those of the heater (about 1 mm $\times$ 1 mm), and the longitudinal dimension is ct_p. In momentum space, phonons are mainly located in a narrow angular distribution.

III. THE KINETIC EQUATION FOR THE DISTRIBUTION FUNCTION OF h-PHONONS

In this section we derive expressions for the rates of increase and decrease of a h-phonon with momentum $\mathbf{p}$ due to 4PP scattering in an equilibrium distribution of l-phonons which is anisotropic. As three-phonon processes are prohibited by conservation laws for h-phonons, the fastest processes which determine the creation rate of h-phonon in l-phonon systems are 4PP. In this process there are two initial phonons and two final phonons. The conservation laws of energy and momentum for 4PP can be written as

$$\varepsilon_1 + \varepsilon_2 = \varepsilon_3 + \varepsilon_4, \quad \mathbf{p}_1 + \mathbf{p}_2 = \mathbf{p}_3 + \mathbf{p}_4. \tag{3}$$

In Eq. (3) and below, the phonon with energy ε_1 and momentum $\mathbf{p}_1$ is the h-phonon and the other three phonons are l-phonons.

The kinetic equation describing the change of the distribution function $n(\mathbf{p}_1) \equiv n_1$ due to 4PP can be written as

$$\frac{dn_1}{dt} = N_b(\mathbf{p}_1) - N_d(\mathbf{p}_1), \tag{4}$$

where $N_b(\mathbf{p}_1)$ and $N_d(\mathbf{p}_1)$ are, respectively, the rates of increasing and decreasing numbers of h-phonons with momentum $\mathbf{p}_1$ due to collisions.

To obtain an explicit expression for $N_{b,d}(\mathbf{p}_1)$ we take l-phonons to be in equilibrium due to the rapid 3PP. Their Bose-Einstein distribution function is[16,11]

$$n_l^{(0)} = \left\{ \exp\left(\frac{\varepsilon_l - \mathbf{p}_l \cdot \mathbf{u}}{k_B T} \right) - 1 \right\}^{-1}, \tag{5}$$

with the drift velocity $\mathbf{u}$, which can be written as

$$\mathbf{u} = \mathbf{N} c(1 - \chi), \tag{6}$$

where $\mathbf{N}$ is the unit vector directed along the direction of the total momentum of the l-phonon system; this defines the anisotropy axis of the phonon system. This equation defines χ, the anisotropy parameter. In weakly anisotropic systems, χ is close to unity. For strongly anisotropic systems, which corresponds to the experiments[1–3] $\chi \ll 1$.

Taking into account the conservation laws [see Eq. (3)] $N_{b,d}$ can be written as

$$N_b = e^{-(\varepsilon_1 - \mathbf{p}_1\cdot\mathbf{u})/k_BT}(1+n_1)\nu_1, \quad N_d = n_1\nu_1, \tag{7}$$

where the 4PP scattering rate is

$$\nu_1(\mathbf{p}_1) = \int d^3p_2 d^3p_3 d^3p_4 n_2^{(0)}(1+n_3^{(0)})(1+n_4^{(0)}) \times W(\mathbf{p}_1,\mathbf{p}_2;\mathbf{p}_3,\mathbf{p}_4)\delta(\mathbf{p}_1+\mathbf{p}_2-\mathbf{p}_3-\mathbf{p}_4) \times \delta(\varepsilon_1+\varepsilon_2-\varepsilon_3-\varepsilon_4). \tag{8}$$

The function $W(\mathbf{p}_1,\mathbf{p}_2;\mathbf{p}_3,\mathbf{p}_4)$, following Refs. 8, 7, and 17, can be written as

$$W(\mathbf{p}_1,\mathbf{p}_2;\mathbf{p}_3,\mathbf{p}_4) = \frac{p_1p_2p_3p_4}{2^{11}\pi^5\hbar^7\rho^2}M^2, \tag{9}$$

where ρ is the density of liquid helium and M is the matrix element for the 4PP, which is calculated to be

$$M = M^{(1)} + M_{13}^{(3)} + M_{23}^{(3)} + M_{14}^{(3)} + M_{24}^{(3)} + M^{(5)} + M_4, \tag{10}$$

where

$$M^{(1)} = \frac{\varepsilon_{1+2}}{\varepsilon_1+\varepsilon_2-\varepsilon_{1+2}}(2u-1+\mathbf{n}_1\cdot\mathbf{n}_2+\mathbf{n}_1\cdot\mathbf{n}_{1+2}+\mathbf{n}_2\cdot\mathbf{n}_{1+2}) \times (2u-1+\mathbf{n}_3\cdot\mathbf{n}_4+\mathbf{n}_3\cdot\mathbf{n}_{3+4}+\mathbf{n}_4\cdot\mathbf{n}_{3+4}), \tag{11}$$

$$M^{(5)} = -\frac{\varepsilon_{1+2}}{\varepsilon_1+\varepsilon_2+\varepsilon_{1+2}} \times (2u-1+\mathbf{n}_1\cdot\mathbf{n}_2-\mathbf{n}_1\cdot\mathbf{n}_{1+2}-\mathbf{n}_2\cdot\mathbf{n}_{1+2}) \times (2u-1+\mathbf{n}_3\cdot\mathbf{n}_4-\mathbf{n}_3\cdot\mathbf{n}_{3+4}-\mathbf{n}_4\cdot\mathbf{n}_{3+4}), \tag{12}$$

$$M_4 = 4\{(u-1)^2+w\}, \tag{13}$$

$$M_{13}^{(3)} = \frac{\varepsilon_{1-3}}{\varepsilon_1-\varepsilon_3-\varepsilon_{1-3}}(2u-1+\mathbf{n}_1\cdot\mathbf{n}_3+\mathbf{n}_1\cdot\mathbf{n}_{1-3}+\mathbf{n}_3\cdot\mathbf{n}_{1-3}) \times (2u-1+\mathbf{n}_2\cdot\mathbf{n}_4+\mathbf{n}_2\cdot\mathbf{n}_{1-3}+\mathbf{n}_4\cdot\mathbf{n}_{1-3}), \tag{14}$$

Other terms of expression (10), i.e., $M_{23}^{(3)}$, $M_{14}^{(3)}$, $M_{24}^{(3)}$ can be obtained from $M_{13}^{(3)}$ by replacement of corresponding subscripts. Here $\mathbf{n}_i = \frac{\mathbf{p}_i}{p_i}$, $\varepsilon_i = \varepsilon(\mathbf{p}_i)$, $u = \frac{\rho}{c}\frac{\partial c}{\partial \rho} = 2.84$ is the Grüneisen constant and $w = \frac{\rho^2}{c}\frac{\partial^2 c}{\partial \rho^2} = 0.188$.

For short pulses that were used in experiments, for example, see Ref. 12, n_1 is much less than the unity and from Eq. (7) we have

$$N_b^{(sh)} = e^{-(\varepsilon_1 - \mathbf{p}_1\mathbf{u})/k_BT}\nu_1. \tag{15}$$

In order to calculate the creation rate N_b and the decay rate N_d, which appear in the kinetic equation (4), we must find the rate ν_1 which is done in the next section.

IV. THE SCATTERING RATE OF *h*-PHONONS IN THE ANISOTROPIC *l*-PHONON SYSTEM

In this section we evaluate the 4PP scattering rate for the *h*-phonons in the anisotropic *l*-phonon system. The general expression for the rate ν_1 is obtained by rewriting the expression (8), taking into account Eqs. (9)–(14), in spherical coordinates and making the integration with respect to φ_3, φ_4 and p_4, θ_4 with the help of the δ functions. As a result we have

$$\nu_1 = \frac{1}{2^{10}\pi^5\hbar^7\rho^2 c}p_1\int dp_2 dp_3 d\zeta_2 d\zeta_3 d\varphi_2 \frac{p_2^3p_3^3p_4^2}{\sqrt{R}} \times (M_{(+)}^2 + M_{(-)}^2)n_2^{(0)}(1+n_3^{(0)})(1+n_4^{(0)}). \tag{16}$$

Here $\zeta_i = 1-\cos\theta_i$, where θ_i is the angle between $\mathbf{p}_i$ and $\mathbf{N}$,

$$p_4 = p_1+p_2-p_3-\phi, \quad \phi = p_3\psi_3+p_4\psi_4-p_1\psi_1-p_2\psi_2,$$

$$\psi_i = \psi(p_i), \tag{17}$$

$$R = 4p_{3\perp}^2p_{4\perp}^2 - (A-p_{3\perp}^2-p_{4\perp}^2)^2, \quad p_{i\perp} = p_i\sqrt{2\zeta_i-\zeta_i^2}, \tag{18}$$

$$A = p_{1\perp}^2 + p_{2\perp}^2 + 2p_{1\perp}p_{2\perp}\cos\varphi_2,$$

$$\zeta_4 = \frac{p_1\zeta_1+p_2\zeta_2-p_3\zeta_3-\phi}{p_4}, \tag{19}$$

$$M_{(\pm)} = M(\cos\varphi_3 = \cos\varphi_3^{(\pm)}, \cos\varphi_4 = \cos\varphi_4^{(\pm)}), \tag{20}$$

$$\cos\varphi_3^{(\pm)} = \frac{(p_{1\perp}+p_{2\perp}\cos\varphi_2)(A+p_{3\perp}^2-p_{4\perp}^2) \pm p_{2\perp}\sin\varphi_2\sqrt{R}}{2Ap_{3\perp}}, \tag{21}$$

$$\cos\varphi_4^{(\pm)} = \frac{(p_{1\perp}+p_{2\perp}\cos\varphi_2)(A-p_{3\perp}^2+p_{4\perp}^2) \mp p_{2\perp}\sin\varphi_2\sqrt{R}}{2Ap_{4\perp}}. \tag{22}$$

We notice that the value of ϕ in the above process is always positive ($\phi>0$). For all further calculations, we shall use the approximation of function $\psi(p)$, obtained in Ref. 8.

Further integration could not be precisely made analytically because of the complicated integrand expression. The dependencies of ν_1 on p_1, ζ_1 and T, χ can only be obtained by numerical integration of Eq. (16). The results of this are shown in Fig. 1. In Fig. 1 is shown the angular dependence of the rate ν_1 at different values of p_1 and fixed values of $T=0.041$ K and $\chi=0.02$. We see that there is a maximum when value of $cp_1/k_B < 13$ K. There are several reasons for this maximum when $cp_1/k_B = 10$ K: first it follows from the conservation laws of energy and momentum that the four-phonon processes are prohibited if the angle between the momenta of phonons $\mathbf{p}_1$ and $\mathbf{p}_2$ is less than

$$\zeta_{12\min} = 1-\cos\theta_{12\min} \approx \frac{p_1+p_2}{p_1p_2}\phi. \tag{23}$$

Secondly the distribution function of phonons in a pulse has a sharp maximum at $\theta_2=0$. Thus, the majority of phonons in a pulse have momentum $\mathbf{p}_2$ directed along the anisotropy axis of the system. However at $\theta_1=0$ phonons with momentum $\mathbf{p}_1$ cannot interact with phonons having momentum $\mathbf{p}_2$

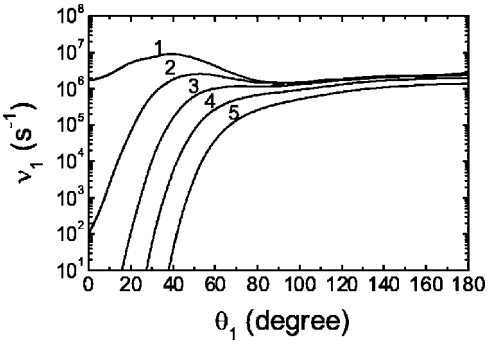

FIG. 1. The 4PP rate ν_1 is shown as a function of the angle θ_1 between p_1 and the propagation direction, calculated from Eq. (16), for different values of cp_1/k_B equal to 10, 11, 12, 13, and 14 K, shown as solid lines 1–5, respectively. All calculations have $T=0.041$ K and $\chi=0.02$.

directed along the anisotropy axis because there is a minimum angle $\theta_{12\min}$ for interaction between them. So the created h-phonon cannot interact with most of the l-phonons in the pulse. With increasing angle θ_1, an increasing number of phonons in the pulse interact with the h-phonon. This leads to the increasing rate in the initial part of the curve, up to $\theta_1 \approx 40°$, see Fig. 1, where the h-phonon can interact with almost all the phonons in the pulse. The decrease in the rate is caused by the decreasing value of the matrix element with increasing angle θ_1. The matrix element is approximately constant after $\theta_1 \sim > \theta_{1\mathrm{ME}} \approx 80°$. Then the slow growth of the rate is determined by the factor R in the integrand of Eq. (16), see Fig. 1.

The situation is different when the momentum p_1 is well above p_c. From Eq. (23) we see that the angle $\theta_{12\min}$ increases with larger p_1 and becomes greater than the angle $\theta_{1\mathrm{ME}}$. Then the rate rises monotonically with increasing θ_1 and there is no range of angles where the rate decreases. This behavior is apparent when $cp_1/k_B \geqslant 13$ K, see Fig. 1.

The dependence of ν_1 on the parameters χ and T is completely determined by the dependence of distribution function $n_2^{(0)}$ on these parameters. So the rate increases with both increasing temperature and with decreasing values of the anisotropy parameter χ.

V. THE ANGULAR DISTRIBUTION OF *l*- AND *h*-PHONONS

The angular distribution of l- and h-phonons can be described by the probability density of the angular distribution of phonons. The probability density of created h-phonons as a function of ζ_1 is defined by expression

$$W_h(\zeta_1,\chi,T) = \frac{\int_{p_c}^{p_{\max}} \varepsilon_1 N_b^{(sh)}(p_1,\zeta_1,\chi,T) p_1^2 dp_1}{4\pi^2\hbar^3 \dot{E}_h}, \quad (24)$$

where

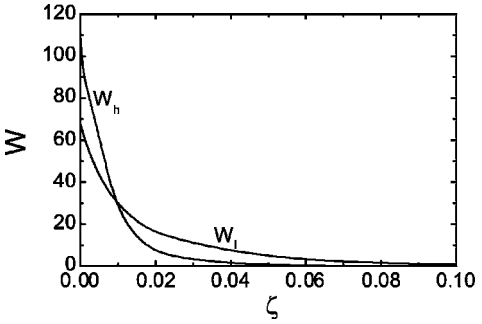

FIG. 2. The angular dependence of the probability density W for the h- and l-phonon distributions at $\chi=0.02$ and $T=0.041$ K, from Eqs. (24) and (26), respectively. Note the angular distribution is narrower for h-phonons than for l-phonons.

$$\dot{E}_h = \frac{1}{4\pi^2\hbar^3}\int_0^2 d\zeta_1 \int_{p_c}^{p_{\max}} \varepsilon_1 N_b^{(sh)}(p_1,\zeta_1,\chi,T) p_1^2 dp_1 \quad (25)$$

is the total energy of h-phonons, created in unit time and unit volume, $N_b^{(sh)}(p_1,\zeta_1,\chi,T)$ is defined by Eq. (15), and the upper limit of integration over momentum $p_{\max}=1.4p_c$ is chosen. The value of the integrals are not sensitive to the exact value of this upper limit as long as it is well above p_c: if $p_{\max}=1.1p_c$ then the later results change very little. The main contribution to the integrals is due to h-phonons with momentum close to p_c because the function $N_b^{(sh)}(p_1)$ rapidly decreases when p_1 increases due to the exponential multiplier in Eq. (15).

Similarly we can also introduce the probability density of l-phonons as a function of ζ_l

$$W_l(\zeta_l,\chi,T) = \frac{\int_0^{p_c} \varepsilon_l n_l^{(0)}(p_l,\zeta_l,\chi,T) p_l^2 dp_l}{4\pi^2\hbar^3 E_l}, \quad (26)$$

where

$$E_l = \frac{1}{4\pi^2\hbar^3}\int_0^2 d\zeta_l \int_0^{p_c} \varepsilon_l n_l^{(0)}(p_l,\zeta_l,\chi,T) p_l^2 dp_l \quad (27)$$

is the total energy of l-phonons in the pulse, in unit volume, and $n_l^{(0)}(p_l,\zeta_l,\chi,T)$ is defined by Eqs. (5), (6).

The results of numerical calculations of W_l and W_h obtained from Eqs. (24) and (26) at $\chi=0.02$ and $T=0.041$ K are given in Fig. 2. We see that W_h is a considerably sharper function of angle than W_l.

The sharpness of functions $W_{l,h}$ is defined by the angular width of the corresponding distributions which are given by relation

$$\bar{\zeta}_{l,h} = \int_0^2 \zeta_{l,h} W_{l,h} d\zeta_{l,h}. \quad (28)$$

Our calculations show the inequality $\bar{\zeta}_h \ll \bar{\zeta}_l$ is satisfied for a wide range of χ and T. Thus the created h-phonons always occupy a narrower cone than the l–phonons. This characteristic was observed in experiments.[18,19] The angluar distribution of the h-phonons had a half width at half maximum

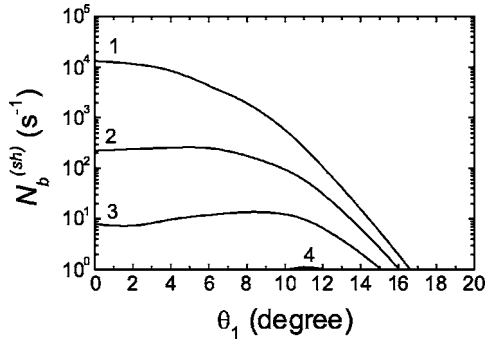

FIG. 3. The creation rate of h-phonons, $N_b^{(sh)}$ in short pulses, is shown as a function of the angle θ_1 between p_1 and the propagation direction, for different values of cp_1/k_B equal to 10, 11, 12, and 13 K, curves 1–4, respectively. All curves have $\chi=0.02$ and $T=0.041$ K.

of 4°, while for l-phonons the half width at half maximum was 11°. The results of calculations, with values of parameters which correspond to ζ_p and T_p (Ref. 16) which are typical for experiments,[18,19] $T=0.041$ K and $\chi=0.02$, give $\bar{\zeta}_l=1-\cos\bar{\theta}_l\approx 0.022$ and $\bar{\zeta}_h=1-\cos\bar{\theta}_h\approx 0.0046$, which correspond to $\bar{\theta}_l\approx 12°$ and $\bar{\theta}_h\approx 5.5°$. These calculated values are in good agreement with the experimental values.

The reasons for the concentration of h-phonons near the anisotropy axis of the system can now be explained as follows. The rapidly decreasing value of W_h with increasing ζ_1, is related to the angular dependence of $N_b^{(sh)}$ which is shown on Fig. 3. It can be seen in Fig. 3, that $N_b^{(sh)}$ very quickly decreases with increasing θ_1. This decrease is determined by the multiplier

$$\exp\left(-\frac{(\varepsilon_1-\mathbf{p}_1\cdot\mathbf{u})}{k_BT}\right)=\exp\left(-\frac{cp_1}{k_BT}(\psi_1+\chi+\zeta_1-\zeta_1\chi)\right) \tag{29}$$

in expression (15), which has a sharp maximum at $\theta_1=0$ when $\chi\ll 1$. So the presence of the exponential multiplier leads to the fast decrease of the function $N_b^{(sh)}(\theta_1)$ when function $\nu_1(\theta_1)$ increases.

VI. THE EVOLUTION OF A SHORT l-PHONON PULSE DUE TO h-PHONON CREATION

In this section we consider how the temperature and the anisotropy of the l-phonons change when energy and momentum is lost from a short pulse due to h-phonon creation. These are characterized by $T(t)$ and $\chi(t)$. We also calculate how the energy, E_l, and the angular width, $\bar{\zeta}_l$, of the pulse change with time. A short phonon pulse is such that all the created h-phonons are lost from the l-phonon pulse well before equilibrium between l- and h-phonons is established. The kinetic equation (4) in this case can be written as

$$\frac{dn_1}{dt}=N_b^{(sh)}. \tag{30}$$

We multiply the right and left part of Eq. (30) by ε_1 and integrate over all $d^3p_1/(2\pi\hbar)^3$. As result we have

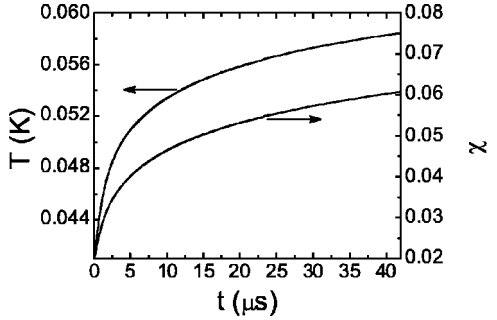

FIG. 4. The anisotropy parameter $\chi(t)$ and temperature $T(t)$ are shown as functions of time, calculated with initial conditions $\chi_0=0.02$, $T_0=0.041$ K.

$$\frac{d\varepsilon_h}{dt}=\dot{E}_h, \tag{31}$$

where $\dot{E}_h$ is defined by expression (25), and

$$\varepsilon_h=\frac{1}{4\pi^2\hbar^3}\int_0^2 d\zeta_1\int_{p_c}^{p_{\max}} dp_1p_1^2\varepsilon_1n_1. \tag{32}$$

From conservation of energy it follows that

$$\frac{d\varepsilon_h}{dt}=-\frac{dE_l}{dt}, \tag{33}$$

where E_l is defined by expression (27). From Eqs. (31) and (33) we have

$$-\frac{dE_l}{dt}=\dot{E}_h. \tag{34}$$

Now we multiply the right and left part of Eq. (30) by p_{1z} and in a similar way obtain

$$-\frac{dP_l}{dt}=\dot{P}_h, \tag{35}$$

where

$$P_l=\frac{1}{4\pi^2\hbar^3}\int_0^2 d\zeta_l\int_0^{p_c} n_l^{(0)}(p_l,\zeta_l,\chi,T)p_l^3(1-\zeta_l)dp_l, \tag{36}$$

$$\dot{P}_h=\frac{1}{4\pi^2\hbar^3}\int_0^2 d\zeta_1\int_{p_c}^{p_{\max}} N_b^{(sh)}(p_1,\zeta_1,\chi,T)p_1^3(1-\zeta_1)dp_1. \tag{37}$$

Thus, we have obtained two equations (34) and (35) that must be solved with respect to functions $\chi(t)$ and $T(t)$ with the initial conditions $\chi(t=0)=\chi_0$ and $T(t=0)=T_0$.

Figure 4 shows the dependencies of χ and T on time t for typical experimental values of $\chi_0=0.02$ and $T_0=0.041$ K. These dependencies were obtained by numerical solution of the combined equations (34) and (35). It can be seen from Fig. 4 that the h-phonon creation leads not only to increasing χ but also to increasing T; nevertheless the total energy density of l-phonon pulse decreases with time.

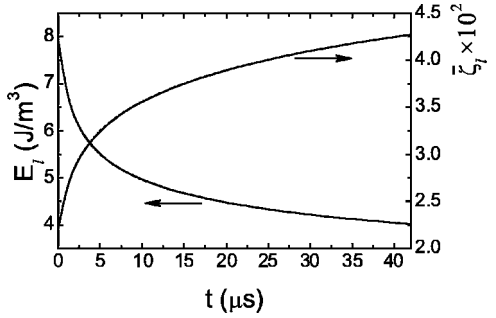

FIG. 5. The l-phonon energy density $E_l(t)$, and the angular width of the l-phonons in momentum space $\bar{\zeta}_l(t)$, are shown as functions of propagation time, calculated with initial values of $\chi_0=0.02$, $T_0=0.041$ K.

In Fig. 5 the time dependence of the l-phonon energy density $E_l(t)=E_l[\chi(t),T(t)]$ and of the l-phonon pulse angular width $\bar{\zeta}_l(t)=\bar{\zeta}_l[\chi(t),T(t)]$ are shown. The broadening of a pulse with time, seen in Fig. 5, is due to the conservation of momentum when h-phonons are created in the l-phonon pulse. The created h-phonons, as can be seen in Fig. 2, have a sharper angular dependence and so they carry away mainly momentum parallel to the anisotropy axis. To compensate for this, the l-phonon angular distribution must broaden. For other values of χ_0 and T_0, all the dependencies are qualitatively the same as shown in the figures.

We introduce

$$\Delta(t)=\frac{E_l(\chi_0,T_0)-E_l[\chi(t),T(t)]}{E_l(\chi_0,T_0)}, \tag{38}$$

which is the fraction of the l-phonon energy which transforms into h-phonons.

In Fig. 6 the function $\Delta(t)$ is shown at $\chi_0=0.02$ for four values of the initial temperature $T_0=0.041$ K, $T_0=0.036$ K, $T_0=0.030$ K, and $T_0=0.025$ K (curves 1–4, respectively). It can be seen from Fig. 6 that the process of h-phonon creation is more rapid at higher values of the initial temperature. The dependence $\Delta(t)$ shown in Fig. 6 is close to that obtained in

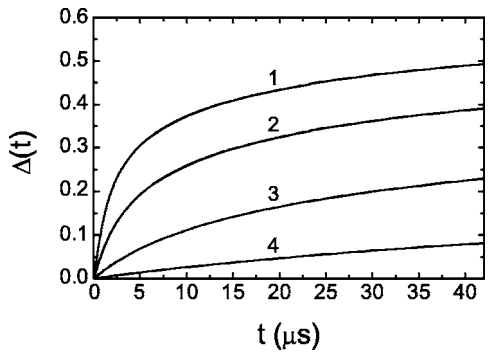

FIG. 6. The energy density lost by the l-phonons, due to h-phonon creation, relative to the initial l-phonon energy density $\Delta(t)$, is shown as a function of time, calculated with $\chi_0=0.02$ for different values of T_0 equal to 0.041, 0.036, 0.030, and 0.025 K, curves 1–4, respectively. When $T_0=0.020$ K the curve lies just above the time axis.

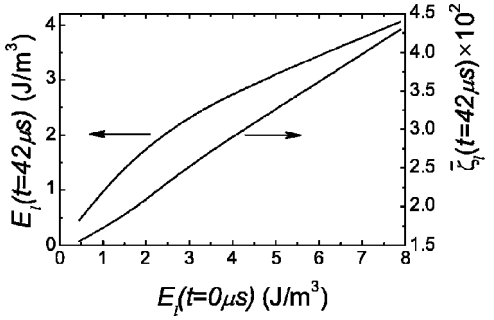

FIG. 7. The l-phonon energy density after 42 μs, $E_l(t=42\ \mu s)$ and angular width of the l-phonons in momentum space after 42 μs, $\bar{\zeta}_l(t=42\ \mu s)$ are shown as functions of the initial l-phonon energy density. All calculations were made with $\chi_0=0.02$.

Refs. 4 and 10, which was derived with the approximate B-E cone distribution function.

In Fig. 7 we show the energy density in the l-phonon sheet after 42 μs as a function of the initial energy density at the heater. This plot corresponds to measuring the energy density in the l-phonons as a function of heater power. Also in Fig. 7 we show the average angle $\bar{\zeta}_l$ at 42 μs as a function of the initial energy density. We see that angular distribution of the l-phonons increases with the initial energy density in the sheet. It also increases with propagation time. From Fig. 7 we see that with increasing heater power, we expect wider and higher energy pulses on the detector. Such behavior was observed in experiments, see Figs. 3 and 7 in Ref. 12.

The behavior shown by the results of this section can only be obtained from the exact distribution function (5) and after rigorous and consecutive calculations. We note that the present theory is only strictly applicable for very wide pulses where we can neglect the transverse evolution of the pulse: in the center of wide pulses there are moving quasiparticles with a uniform temperature. Neglecting the spatial evolution of the pulse, during its motion from the heater to the detector, is not expected to change the qualitative behavior derived in this section, although the quantiative results will change.

The spatial evolution of cold l-phonon pulses, where the creation of h-phonons can be neglected, was considered in Refs. 20 and 21. We hope that combining h-phonon creation and expansion will lead to an explanation of the unusual experimental results reported in Ref. 12 where the angular variation of the l-phonon signal had a mesa shape, i.e., the phonon sheet had a central area where the energy density was constant.

VII. CONCLUSION

In this paper the creation and decay processes of high-energy phonons in anisotropic low-energy phonon systems have been investigated. We obtained the general expression for the 4PP rate ν_1, which describes the creation and decay processes of high-energy phonons. It applies at any angle to the anisotropy axis of the system, and for different values of temperature T and parameter of anisotropy χ [see Eq. (16)].

The dependencies of the rate $\nu_1(p_1,\zeta_1,\chi,T)$ on all parameters were calculated numerically starting from Eq. (16).

Also the physical reasons of these dependencies (see Fig. 1) were analyzed.

Calculation of the rate ν_1 has allowed the angular distribution of the created *h*-phonons and *l*-phonons to be determined (see Fig. 2). As a result it was shown that the solid angle, occupied by created *h*-phonons in momentum space, is always less than the solid angle occupied by the *l*-phonons. It allowed us to explain (see Figs. 2 and 3) why the *h*-phonons are concentrated around the anisotropy axis of the system, as observed experimentally in Ref. 2.

Starting from the kinetic equation (30), the problem of the evolution of a short *l*-phonon pulse, due to the creation of *h*-phonons, was solved. The time dependencies of the temperature T and the parameter of anisotropy χ (see Fig. 4) were found. It allowed us to obtain the dependence of the *l*-phonon energy on time and to show that the creation of *h*-phonons leads to broadening of the *l*-phonon pulse (see Figs. 5 and 6). These calculated dependencies (see Fig. 7) also explained the measured dependence of the detected *l*-phonon signal amplitude on the heater power: how the *l*-phonon signal amplitude increases with heater power (see Fig. 7 of Ref. 12).

ACKNOWLEDGMENTS

We express our gratitude to EPSRC of the UK (Grant No. EP/C 523199/1) for support of this work.

*Email address: a.f.g.wyatt@ex.ac.uk

[1] A. F. G. Wyatt, N. A. Lockerbie, and R. A. Sherlock, J. Phys.: Condens. Matter **1**, 3507 (1989).
[2] M. A. H. Tucker and A. F. G. Wyatt, J. Phys.: Condens. Matter **6**, 2813 (1994).
[3] M. A. H. Tucker and A. F. G. Wyatt, J. Low Temp. Phys. **113**, 621 (1998).
[4] I. N. Adamenko, K. E. Nemchenko, A. V. Zhukov, M. A. H. Tucker, and A. F. G. Wyatt, Phys. Rev. Lett. **82**, 1482 (1999).
[5] S. Havlin and M. Luban, Phys. Lett. **42**, 133 (1972).
[6] M. A. H. Tucker, A. F. G. Wyatt, I. N. Adamenko, A. V. Zhukov, and K. E. Nemchenko, Low Temp. Phys. **25**, 488 (1999) [Fiz. Nizk. Temp. **25**, 657 (1999)].
[7] M. A. H. Tucker and A. F. G. Wyatt, J. Phys.: Condens. Matter **4**, 7745 (1992).
[8] I. N. Adamenko, K. E. Nemchenko, and A. F. G. Wyatt, J. Low Temp. Phys. **125**, 1 (2001).
[9] I. N. Adamenko, K. E. Nemchenko, and A. F. G. Wyatt, J. Low Temp. Phys. **126**, 1471 (2002).
[10] A. F. G. Wyatt, M. A. H. Tucker, I. N. Adamenko, K. E. Nemchenko, and A. V. Zhukov, Phys. Rev. B **62**, 9402 (2000).
[11] I. N. Adamenko, Yu. A. Kitsenko, K. E. Nemchenko, V. A. Slipko, and A. F. G. Wyatt, Phys. Rev. B **72**, 054507 (2005).
[12] R. V. Vovk, C. D. H. Williams, and A. F. G. Wyatt, Phys. Rev. B **68**, 134508 (2003).
[13] H. J. Maris and W. E. Massey, Phys. Rev. Lett. **25**, 220 (1970).
[14] W. G. Stirling, in 75th *Jubilee Conference on Liquid Helium-4*, edited by J. G. M. Armitage (World Scientific, Singapore, 1983), p. 109.
[15] I. N. Adamenko, K. E. Nemchenko, V. A. Slipko, and A. F. G. Wyatt, J. Phys.: Condens. Matter **17**, 1 (2005).
[16] I. N. Adamenko, Yu. A. Kitsenko, K. E. Nemchenko, V. A. Slipko, and A. F. G. Wyatt, Low Temp. Phys. **31**, 459 (2005) [Fiz. Nizk. Temp. **31**, 607 (2005)].
[17] I. M. Khalatnikov, *An Introduction to the Theory of Superfluidity* (Addison-Wesley, Redwood City, CA, 1989).
[18] M. A. H. Tucker and A. F. G. Wyatt, J. Phys.: Condens. Matter **6**, 2825 (1994).
[19] M. A. H. Tucker and A. F. G. Wyatt, Physica B **194**, 551 (1994).
[20] I. N. Adamenko, K. E. Nemchenko, V. A. Slipko, and A. F. G. Wyatt, Phys. Rev. B **68**, 134507 (2003).
[21] I. N. Adamenko, K. E. Nemchenko, V. A. Slipko, and A. F. G. Wyatt, J. Low Temp. Phys. **138**, 67 (2005).